

Gas Adsorption and Separation in Realistic and Idealized Frameworks of Organic Pillared Graphene: A Comparative Study

Giovanni Garberoglio,^{*,†,‡} Nicola M. Pugno,^{§,||,⊥} and Simone Taioli^{*,†,‡}

[†]European Centre for Theoretical Studies in Nuclear Physics and Related Areas (ECT*), Bruno Kessler Foundation, Trento, Italy

[‡]Trento Institute for Fundamental Physics and Applications (INFN-TIFPA), Trento, Italy

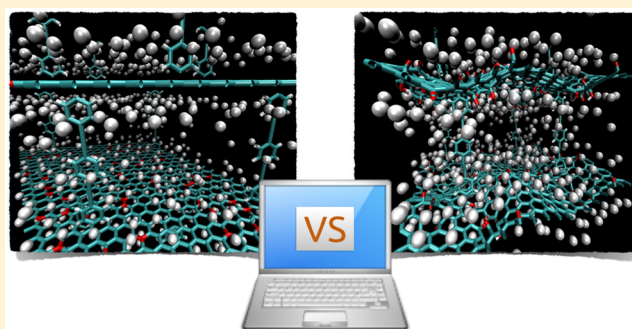
[§]Laboratory of Bio-Inspired & Graphene Nanomechanics, Department of Civil, Environmental, and Mechanical Engineering, University of Trento, Trento, Italy

^{||}Center for Materials and Microsystems, Fondazione Bruno Kessler, Trento, Italy

[⊥]School of Engineering and Materials Science, Queen Mary University of London, London E1 4NS, United Kingdom

S Supporting Information

ABSTRACT: In this work, we present a systematic and thorough comparison between gas adsorption and energy storage properties in idealized or realistic models of organic-pillared reduced-graphene-oxide sheets. First, atomistic simulations based on density functional theory are used to generate the structures of these novel systems. Second, Grand Canonical Monte Carlo is used to predict the adsorption properties of the proposed frameworks in the case of two different gases, notably hydrogen and carbon dioxide. While one can safely conclude that gas adsorption is strongly affected by the density of the pillars and the chemical composition of the compounds, a comparison between realistic idealized structures shows that even the corrugation of graphene sheets has a deep impact on such properties. Finally, we produce evidence of the potentiality of these pillared structures to be used as gas separation devices by investigating the sieving of an equimolar CO₂/H₂ mixture at room temperature.



■ INTRODUCTION

In recent years, there has been ever growing interest in technological applications of graphene-based compounds, with numerous groups succeeding in harnessing the peculiar characteristics of this material.

One of the most notable uses of graphene is to produce carbon-based devices by exploiting its unsurpassed electronic properties.^{1–5} In this respect, the interaction of small molecules with graphene has been studied in detail for tuning its electronic and optical properties, with particular emphasis to hydrogen.^{6,7} However, due to the large available area, the study of graphene hydrogenation and physisorption^{8–10} may be interesting also as a prototype of hydrogen storage in carbon materials.¹¹

To develop graphene-based nanostructures for storage purposes, it is convenient to start from the oxidized form of graphene, which is soluble as well as has better reactivity than CVD-graphene.¹² Graphene-oxide (GO) based membranes have been shown to have very interesting properties for fluid treatment, such as an exceptional selectivity for water¹³ and a promising chemisorption¹⁴ or physisorption¹⁵ capacity for hydrogen storage.

In order to exploit extensively these unique properties for fluid treatment, GO needs to be arranged in a three-

dimensional framework from its inherently bidimensional structure. One promising route is to insert spacers between GO layers. This procedure leads to a series of materials generally known as pillared graphene-oxide frameworks (PGOFs). To the best of our knowledge the first attempts in this direction were made by Burress and co-workers,^{16,17} using boron-containing compounds as spacers. Recently, Kumar and co-workers showed how to synthesize PGOFs using organic linkers only.¹⁸ The possibility of varying the type of linker and their density paves the way to the rational development of PGOFs with tailored properties.¹⁹ Gas adsorption properties of PGOFs were experimentally characterized and found to be comparable with that of other nanoporous materials, such as metal–organic frameworks (MOFs).²⁰

Recently, various groups have been using a systematic approach to screen large classes of possible MOFs using computer simulations, with the aim of identifying those more suited to gas storage applications.^{21–23} In these investigations, the availability of an accurate and transferable description for the adsorbate–adsorbent interaction has been proven crucial.

Received: December 1, 2014

Revised: December 27, 2014

Published: December 29, 2014

In the case of MOFs, computer modeling is essential to gain microscopic insights on the mechanisms of adsorption (and/or diffusion) and enable a precise characterization of adsorption sites, providing important clues regarding the optimization of the properties for specific tasks.^{24–26}

However, no systematic modeling approach to PGOFs has been reported to date. The principal reason for this lack is that computational investigations are made cumbersome by the nonperiodicity of the atomic structure of the reduced-GO-based (rGO) materials. Burrell et al. performed simulations using idealized models of PGOFs, in order to assess the effect of pillar density on the amount of hydrogen adsorbed.¹⁶ In particular, the graphene-oxide sheets were approximated with planar graphene sheets. A similar approach was adopted by Nicolai and co-workers in their numerical investigation of water diffusion in PGOFs.^{27,28}

Remarkably, no systematic assessment of the quality of these assumptions has been performed to date. The goal of this work is thus to gain real insights into the hydrogen adsorption properties of PGOFs by comparing the results of idealized, as previously done, and realistic models. The same analysis will be repeated for a different gas, notably carbon dioxide. Furthermore, the gas separation properties of the CO₂/H₂ mixture in this structure will be investigated.

In the first part of this manuscript we describe our quantum chemical approach leading to the generation of realistic PGOF structures with atomic-level detail. Our efforts have been inspired by the recent fully organic PGOFs synthesized by Kumar et al.,¹⁸ for which no computational model has been developed so far. In the second part, we present our results on the adsorption of hydrogen and carbon dioxide in PGOFs, comparing the results with idealized models. Finally, gas separation for the CO₂/H₂ mixture is discussed.

■ MODELING PILLARED GRAPHENE-OXIDE FRAMEWORKS AND GAS ADSORPTION THEREIN

Structure Generation. Reduced graphene-oxide is mostly obtained by oxidation of a pristine graphene sheet using a mixture of sulfuric acid, sodium nitrate, and potassium permanganate, following a class of methods proposed by Hummers and Offeman.^{29,30} In this process, oxygen reacts in an uncontrolled manner, thus creating a highly defective and amorphous material. In general, the interaction of oxygen with graphene results in dangling hydroxyl (OH) groups or in epoxide functional groups (oxygen atoms bridging two C atoms of the graphene sheets).^{31,32} In this process, some carbon atoms are removed, leaving defects on the surface.¹² Reduced graphene-oxide is generally characterized by the percentage of oxygen atoms present in the final product, typically ranging from 8% to 25% in number.³⁰

With the further goal of studying the respective adsorption and separation properties, we generated four different structures using atomistic simulations based on classical molecular mechanics (MM), density functional theory (DFT), and its tight-binding approximation (DFTB). This latter approach has been shown to be a very good compromise between accuracy and speed in the calculation of many properties of MOFs.^{33–37}

In order to generate a chemically meaningful PGOF model structure, we started from a pristine graphene layer, using the program Avogadro³⁸ to substitute some randomly chosen carbon atoms with oxygen, making them either bridging oxygen atoms or protruding hydroxyl groups. The number of

substituted oxygen atoms was chosen in order to have a coverage of 10% to 15% of the final graphene-oxide layer.¹⁸ These rGO structures have been initially minimized using the MMFF94 force field³⁹ and further optimized with the DFTB+ program, implementing an efficient tight-binding approximation to DFT.⁴⁰ This step is necessary to describe the formation and disruption of bonds in the oxygen-rich carbon systems.

We used a 0.5 fs time step and a Nosé–Hoover thermostat sampling a NVT ensemble. The target temperature of the thermostat was set to 1500 K for 100 ps and reached by specifying a temperature profile as follows. Temperature was linearly increased from 10 to 1500 K in 400 fs after an initial equilibration of 150 fs at a constant temperature of 10 K. The annealing, at the target temperature, was kept for 100 ps until structural equilibration. Byproducts, mainly consisting of CO molecules, obtained during these annealing periods were deleted. Finally, temperature was exponentially decreased to 10 K in 150 fs.

The rGO structures obtained were further relaxed by using DFT as implemented in the total-energy and molecular dynamics VASP code,⁴¹ with an implementation of an efficient extrapolation for the electronic charge density.⁴² The ion–electron interaction has been described using the projector augmented wave (PAW) technique with single-particle orbitals expanded in plane waves with a cutoff of 400 eV. The Perdew–Burke–Ernzerhof (PBE) exchange–correlation potential⁴³ has been used to treat the electron–electron Coulomb interaction. In all DFT relaxation simulations, electronic and ionic temperature was fixed at 300 K with a corresponding Fermi smearing of the electronic density. The Brillouin zone was sampled at the Γ point only. The rGO structures optimized via DFT were included in a supercell of $22 \times 21 \text{ \AA}^2$ in the lateral dimension and 20 \AA in the direction orthogonal to the graphene sheet to avoid spurious interactions among periodic images. After DFT relaxation, a 2×2 supercell in lateral dimension was created by periodically repeating the DFT supercell and reoptimized using DFTB. DFTB optimizations were performed using the self-consistent charge approach, using the matsci parametrization for the Slater–Koster tables.⁴⁴ Even in this case we sampled the Brillouin zone at the Γ point only. Finally, four organic linkers and a second different 2×2 (obtained as previously) rGO sheet on the top of them were added to generate the three-dimensional superstructure reported in Figure 1. The coordinates of this optimized structure are provided as Supporting Information.

The first set of four linkers was added by creating chemically reactive sites (e.g., by removing a C atom) on a previously optimized rGO sheet already presenting crests and troughs. Pillars were rooted at the position of the chemically active sites. In this way, we favored the formation of covalent bonds with the linkers. This procedure has been repeated again for an independently generated and optimized second layer. We carefully placed the pillars to ensure that a periodic bilayer structure was generated. The geometry so obtained was finally relaxed using DFTB.

Since the density of linkers in the materials synthesized in ref 18 was not specified, we used four linkers, with a final density of 0.2 linkers/nm². We report the principal characteristics of the four structures in Table 1.

The most striking feature of the realistic PGOF model is the fact that the rGO sheets are considerably buckled, with the appearance of crests and troughs. This peculiarity of the actual systems is completely neglected in the idealized modeling used

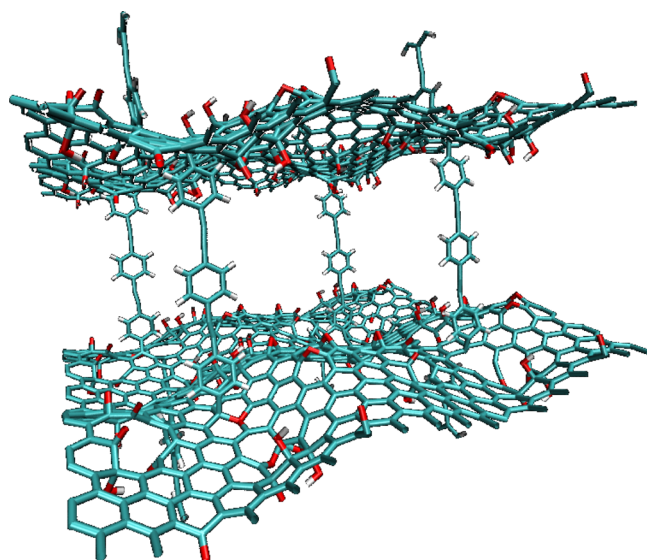


Figure 1. PGO structure considered in this paper. Carbon, oxygen, and hydrogen atoms are colored in green, red, and white, respectively.

Table 1. Principal Characteristics of the PGOFs Modeled in This Work^a

name	oxygen %	volume (Å ³)	free volume (Å ³)	mass (amu)
PGOF-1	10	72442	54470	21811
flat model	10	80998	64571	20970
PGOF-2	10	87965	69692	22419
PGOF-3	15	76137	57613	22633
PGOF-4	15	91661	72415	23270

^aThe “flat model” is an idealized model of PGOF-1. The free volume is defined in eq 1.

so far in the literature and, as we will show below, does have a considerable impact on the prediction of the amount of gas adsorbed in these structures.

Simulation of Gas Adsorption. We performed computer simulations of gas physisorption, notably hydrogen and carbon dioxide, in the optimized structures described in the previous section using standard force fields to model the adsorbate–adsorbent interaction. Molecular hydrogen is representative of those molecules having mainly van der Waals interactions with the adsorbent. In general, it turns out that molecular hydrogen can be effectively modeled as being a single Lennard-Jones center of force, with parameters given by $\epsilon/k_B = 34.2$ K and $\sigma = 2.96$ Å.⁴⁵

In contrast, carbon dioxide is characterized by a quite significant electric quadrupole moment, and electrostatic interactions have to generally be included in any successful model. We decided to use the EPM2 parametrization for the CO₂ molecule, which is made by Lennard-Jones centers and partial charges.⁴⁶

The framework atoms have also been described as Lennard-Jones centers. Two force fields are being generally used in this case: DREIDING⁴⁷ or the Universal Force Field,⁴⁸ the former generally performing slightly better than the second,^{26,49,50} and we decided to use it in our calculations, adopting the Lorentz–Berthelot mixing rules to calculate the interaction between unlike atoms. When simulating carbon dioxide, we considered also electrostatic effects by adding the electrostatic potential produced by partial charges on the framework atoms. These

partial charges were calculated through a Mulliken population analysis from the DFTB calculations.

Adsorption simulations were performed using standard Grand Canonical Monte Carlo (GCMC) techniques. The chemical potential was related to the pressure of the reservoir gas using the van der Waals equation of state, whose parameters have been set to reproduce the position of the adsorbate critical point. For each external pressure we performed 1 million equilibration steps (one step being either an insertion, a deletion, or translation/rotation of an already adsorbed molecule), followed by 5 million production steps. One configuration every thousand was saved for off-line analysis.

When simulating hydrogen adsorption at cryogenic temperatures ($T = 77$ K) quantum diffraction is not negligible.⁴⁹ In principle, the path-integral formulation of quantum mechanics⁵¹ would enable one to describe quantum effects in an accurate manner.^{52–54} Nevertheless, the centroid approximation to the path integral⁵⁵ was shown to be remarkably accurate at this temperature and thus has been adopted in this work. This approximation, that can be derived from quantum statistical mechanics, describes the position of a quantum particle of mass m in thermal equilibrium as being distributed with a Gaussian probability having a variance given by $\sigma^2 = \beta\hbar^2/(12m)$.

The following analysis will be focused on the calculation of the excess amount, N_{ex} , for a given adsorbate species. N_{ex} can be obtained by estimating the number density $\rho(T, P)$ of the adsorbate at the given thermodynamic condition (which we calculate using the van der Waals equation of state) and the available free volume for adsorption, V_{free} . V_{free} is conventionally defined as the volume of the region where the solid–fluid interaction between the framework and a helium atom divided by the Boltzmann constant k_B is less than 10^4 K. This pore volume definition agrees with experimental measurements of adsorption, requiring the helium dead space for volumetric measurements and the buoyancy of the solid in helium for gravimetric measurements.⁵⁶ We modeled the He atom as a Lennard-Jones center with $\epsilon/k_B = 10.22$ K and $\sigma = 2.556$ Å. Finally, the number of adsorbed molecules is given by

$$N_{\text{ex}} = N - \rho(T, P)V_{\text{free}} \quad (1)$$

where N is the total number of gas molecules.

RESULTS AND DISCUSSION

Adsorption of Hydrogen. Hydrogen adsorption isotherms at $T = 77$ K are shown in Figure 2 for the four PGOFs

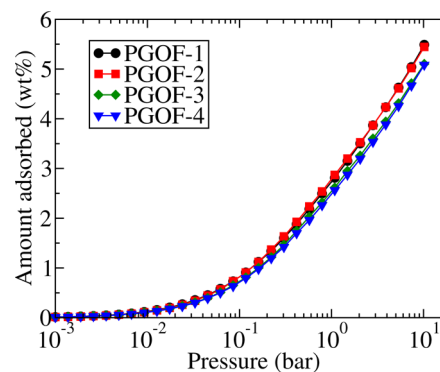


Figure 2. Isotherms of hydrogen adsorption at $T = 77$ K in the PGOFs modeled in this work.

considered in this work. In the range of pressures covered in our investigation, we do not see any tendency of the isotherms to show a saturation behavior. In fact, inspection of the computer-generated configurations shows that at $P = 10$ bar hydrogen accumulates on the GO sheets, with only a small amount to be found in the space within the sheets or in contact with the pillars.

We notice that at low pressures all the PGOFs present a quite similar behavior. In fact, in this regime the isosteric heat of adsorption is roughly 5.7 kJ mol^{-1} , irrespective of the framework investigated.

It is only at high pressure that the differences between the frameworks become apparent: the frameworks PGOF-1 and PGOF-2, with less content of oxygen than PGOF-3 and PGOF-4, adsorb more hydrogen than the other two.

The amount of hydrogen adsorbed in PGOFs at $T = 77 \text{ K}$ is comparable with the amount that is observed, with both experiments and computer simulations, in many MOFs²⁶ and covalent organic frameworks.⁵⁷ However, the experimental results reported in ref 18 seem to indicate that PGOFs should adsorb a significantly smaller amount, roughly by a factor of 3 at $P = 10$ bar. Unfortunately, a direct comparison between our calculations and the data reported in ref 18 is difficult to make, mostly because Kumar et al. do not estimate the density of linkers nor the percentage of oxygen in their samples. Our results are quite close to the one reported by Burrell and co-workers in a similar material.¹⁶ We also notice that Burrell and co-workers study the amount of hydrogen adsorbed as a function of the linker density, finding a significant variation. Thus, one can argue that a linker density larger than ours in the samples investigated in ref 18 could safely explain the discrepancies observed.

Adsorption of Carbon Dioxide. The adsorption isotherms of carbon dioxide at $T = 195 \text{ K}$ are shown in Figure 3

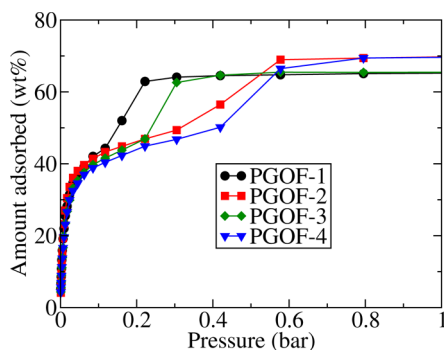


Figure 3. Isotherms of CO_2 adsorption at $T = 195 \text{ K}$ in the PGOFs modeled in this work.

for the four PGOFs considered in this work. These isotherms have a qualitatively different shape than the hydrogen adsorption isotherms, displaying a pronounced step. The presence of this step is commonly observed in computer simulations of CO_2 adsorption (roughly at the same pressure and temperature as in our case) and is due to the fact that beyond a certain density of adsorbed molecules the relatively strong quadrupolar electrostatic interaction between CO_2 molecules further enhances the adsorption, producing the step in the isotherm.⁵⁸

The pressure where the step is observed differs for all the PGOFs investigated here. This suggests that its position

depends on both the oxygen density and the kind of pillar. Experimental data reported in ref 18 do not show the presence of a stepped behavior in the same range of pressure analyzed here. As already discussed in the case of H_2 adsorption, this difference might be attributed to a different density of pillars and/or a different oxygen composition between our models and the actual samples. Nevertheless, we point out that, differently from what has been observed in the case of hydrogen adsorption, the amount of CO_2 adsorbed in our simulations ($\sim 60 \text{ wt} \%$) is comparable with the experimental results.

Comparison with an Idealized Model. In a previous work,¹¹ Tozzini and Pellegrini showed that the corrugation of graphene sheets can strongly influence the hydrogen chemisorption. In order to check the possible effects of corrugation in our case (physisorption), we generated an idealized model of PGOF-1 by considering two ideal graphene sheets separated by a distance appropriate to contain the same linker as the PGOF-1 structure. On the two graphene sheets, 10% of the carbon atoms (chosen randomly) were substituted with oxygen atoms. We emphasize that this idealized model is only an approximation to the realistic one described above. In particular, the atomic positions and the topology of the system are not equal, although they are comparable. On each oxygen atom, we placed a partial charge equal to the average value of the oxygen partial charges in the DFTB+ calculations, $q_{\text{O}} = -0.36|e|$, where e is the electron charge. In order to ensure charge neutrality, we placed a compensating charge $q_{\text{C}} = 0.12|e|$ on the three neighbors of the oxygen atoms. Given the random distribution of the oxygen centers within the graphene sheet, this procedure was not enough to ensure charge neutrality because it might happen that two oxygens were nearest neighbors. In this case, the oxygen charge was left untouched and the remaining compensating charge distributed equally among the carbon atoms near the oxygen atoms. The geometrical parameters of the resulting structure are reported in Table 1.

Computer simulation of hydrogen and oxygen adsorption were performed in the same way as with the other PGOFs. The adsorption isotherms of H_2 at $T = 77 \text{ K}$ and of CO_2 at $T = 195 \text{ K}$ for the idealized structures are reported in Figures 4 and 5, respectively, along with a comparison to the realistic case.

Two features are strikingly evident by analyzing these curves. The first is the slight tendency of the realistic model to adsorb more gas at low pressure (that is, low coverage regime). In this regime, the amount adsorbed is indeed determined by the solid–fluid potential energy surface. This tendency could be

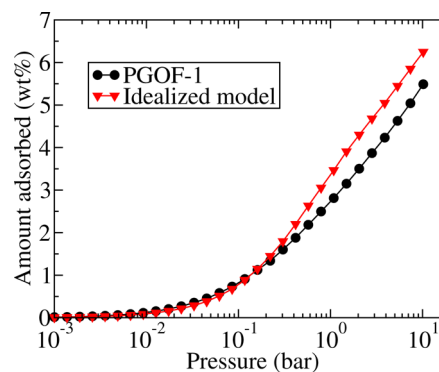


Figure 4. Adsorption isotherm of H_2 at $T = 77 \text{ K}$ in PGOF-1 (circles) and in the idealized model (triangles).

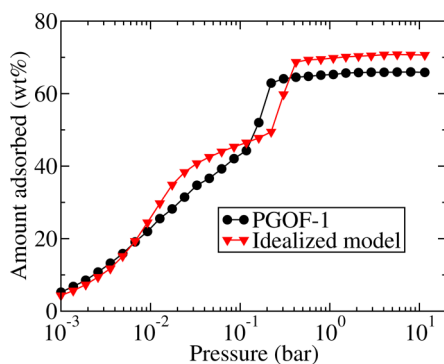


Figure 5. Adsorption isotherm of CO₂ at $T = 195$ K in PGOF-1 (circles) and in the idealized model (triangle).

thus easily explained by the presence of troughs in the buckled graphene sheets of the realistic model, providing adsorption sites with a slightly higher interaction energy with the adsorbate, due to the favorable superposition of the attractive wells of the Lennard-Jones potential.

In the case of hydrogen, we observe a minimum energy of the idealized structure (indicated as idealized model in Figure 4) equal to $V_{\text{flat}}/k_B = -871$ K, to be compared with the minimum energy for the interaction with PGOF-1 which is $V_{\text{PGOF-1}}/k_B = -1057$ K. However, this favorable energetics is contrasted by the relatively small region where the solid–fluid potential attains its minimum, resulting in a modest increase of the amount adsorbed due to the effect of curvature.

At higher pressures, the situation is markedly different. The flat model results in a higher adsorption for both hydrogen and carbon dioxide. In the case of H₂, the amount adsorbed by the flat model is $\sim 14\%$ higher than the amount adsorbed by the realistic PGOF-1 model. In the case of CO₂, the amount adsorbed is as high as $\sim 20\%$. The origin of this difference cannot be attributed to the difference in the unit cell volume (as reported in Table 1). In fact, the quantity used in the comparison—the weight percent of gas adsorbed—is intensive, thus not proportional to the mass of the unit cell. Indeed, an analysis based on the volumetric density of states⁴⁹ corroborates this finding.

Taking hydrogen as a showcase, the average solid–fluid potential energy at the highest pressure investigated is comparable in the two models (-452 K for PGOF-1 and -448 K for flat model), as is the fluid–fluid potential energy per molecule (-52 K for PGOF-1 and -55 K for the flat model). Hence, the different amount of adsorbed molecules must be due to the fact that the fraction of the volume of the unit cell where the solid–fluid potential energy results lower than ~ -450 K is larger for the flat model than for the realistic one.

The volume fraction having energy less than a certain amount is shown in Figure 6 for the realistic and the flat model. Again, one can notice that the realistic model has a larger volume available at the lowest energy (that is, around -600 K), which explains the larger adsorption at low pressure. When one considers the volume fraction where the energy is less than the measured solid–fluid potential at the highest pressure (that is, around -450 K), the trend is opposite. The flat model has a 15% larger volume fraction with solid–fluid interaction energy lower than -450 K and hence is capable of adsorbing more gas. One could then expect an adsorbed amount correspondingly

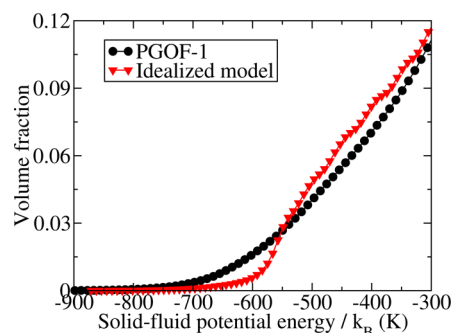


Figure 6. Fraction of unit-cell volume with solid–fluid energy less than a given value. Circles: PGOF-1. Triangles: flat model.

higher, which is indeed in good agreement with the results of the GCMC simulations.

It is interesting to notice that at 10 bar of pressure hydrogen is mostly found adsorbed close to the GO sheets and has not yet occupied the whole available volume, as can be seen in the snapshots reported in Figure 7. A similar distribution is observed for CO₂ in the region around 20 mbar where the amount adsorbed in the flat model is considerably higher than the amount adsorbed in the realistic one.

It is tempting to attribute also this different behavior to the corrugation of the graphene sheets. When compared to the perfectly flat GO sheets, the presence of concavities results in (small) regions with a smaller (more negative) interaction potential, hence a slightly larger adsorption at low external pressures. Conversely, close to the troughs of the realistic GO sheet, the solid–fluid potential energy is higher (less negative) than it would be in the perfectly flat situation. As a consequence of this corrugation, the volume fraction with favorable adsorption energy is smaller in the realistic sheet than in the perfectly flat one, resulting in a smaller amount of gas adsorbed. This different adsorption could be used for instance to selectively release hydrogen as a result of a mechanical deformation.

CO₂/H₂ Selectivity. We also investigated the selectivity of PGOFs for both the realistic and idealized model, in the case of a binary mixture made by carbon dioxide and hydrogen. The selective adsorption of CO₂ from this mixture is an important step in the precombustion treatment of biogases.^{50,59} In the following, the selectivity of an adsorbent for a mixture of gases is defined by the ratio

$$S(b/a) = \frac{x_b/x_a}{y_b/y_a} \quad (2)$$

where x_a denotes the molar fraction of the adsorbed species a and y_a the molar fraction of the same species in the bulk mixture in contact with the adsorbent (with a similar definition for the specie b). Values of $S(b/a)$ greater than one mean that the species b is preferentially adsorbed with respect to the species a .

Our results, reported in Figure 8, show that the pressure dependence of the CO₂/H₂ selectivity at $T = 298$ K displays a similar trend for both the realistic and the idealized PGOF models. The selectivity remains constant up to roughly 1 bar of pressure, where it decreases and then increases again. The last points hint at a further decrease.

This trend, and the actual value of the selectivity between 50 and 60, are analogous to what has been observed for the same mixture, in the case of adsorption in MOFs^{60,61} or in zeolitic

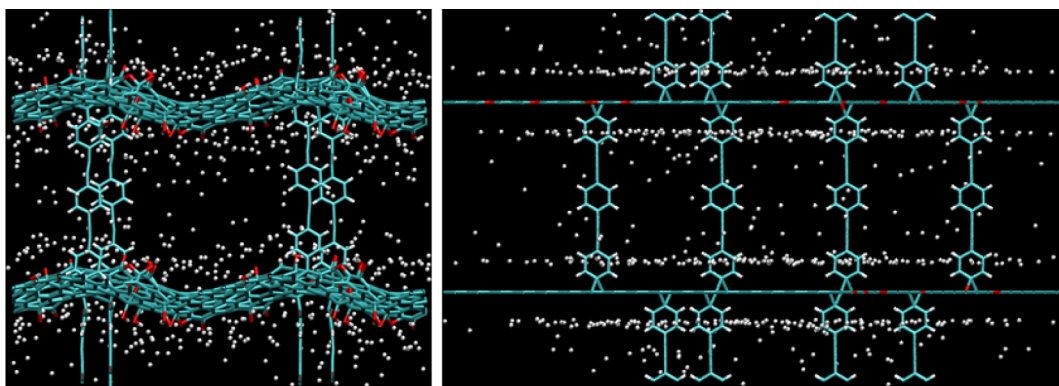


Figure 7. Simulation snapshots showing the typical distribution of hydrogen molecules (represented by white circles) adsorbed in PGOF-1 (left) and the flat model (right), at $T = 77$ K and $P = 10$ bar.

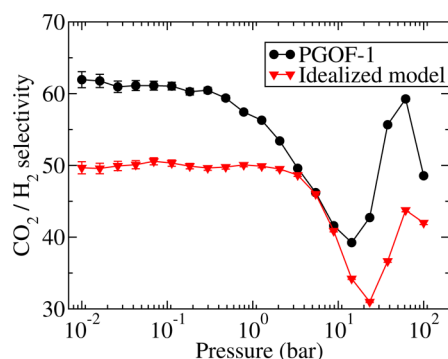


Figure 8. Pressure dependence of the CO_2/H_2 selectivity for an equimolar mixture at $T = 298$ K for PGOF-1 (circles) and its idealized model (triangles).

imidazolate frameworks.⁶² At low pressures (below ~ 0.5 bar) the selectivity is constant. In this regime, the adsorbed gas is so dilute that the value of $S(\text{CO}_2/\text{H}_2)$ is mostly determined by interaction with the substrate. Since the interaction energy of CO_2 is larger than that of H_2 , $S(\text{CO}_2/\text{H}_2)$ is larger than one. At higher pressures, the selectivity starts decreasing due to entropic effects dependent on the smaller size of the hydrogen molecule with respect to carbon dioxide, as discussed in detail by Yang and coauthors.⁶¹ As the pressure is raised, however, the mutual influence between adsorbed molecules becomes appreciable, and the larger $\text{CO}_2\text{--CO}_2$ interaction favors the adsorption of carbon dioxide, resulting in an increase of the selectivity. At higher pressure still, entropy again favors hydrogen, and the selectivity decreases. In the case of the selectivity, the principal difference between the realistic and idealized model is that the latter would predict a value of $S(\text{CO}_2/\text{H}_2)$ smaller by roughly 15%.

CONCLUSIONS

In this paper, we presented computer simulation results of gas adsorption and separation in recently synthesized pillared graphene-oxide frameworks.

Using quantum chemical methods, we developed a realistic model of the framework, reproducing the observed oxygen density of the GO sheets, as well as all the various defects that oxidation produces in pristine graphene sheets. The optimized structures show that the presence of pillars results in a considerable corrugation of the GO sheets.

Computer simulation of hydrogen adsorption shows that the performance of these structures at cryogenic temperatures is

comparable to that of metal organic frameworks. When compared to the available experimental data, likely obtained with PGOFs having a different pillar density than the one we modeled, our results show that there is large room for improving the amount of hydrogen that can be stored, possibly by a factor between two and three.

Conversely, computer simulations of carbon dioxide adsorption are comparable with the experimental data, although in our case pore condensation is observed at the highest pressure investigated. This difference might again be ascribed to the different density of pillars between the model and the actual samples.

Furthermore, we tested the reliability of the widely used idealized models for these structures, built by simple juxtaposition of planar GO sheets and rigid linkers without any further quantum mechanical optimization of the resulting structures.

The idealized models slightly underestimate the amount of gas adsorbed at low coverage but significantly overestimate it (by 15–20%) in the region just before saturation, i.e., when the gas molecules are adsorbed in the proximity of the GO sheets. This difference has been related to the corrugation of the GO planes.

Finally, we investigated the effect of modeling on the adsorptive separation of a CO_2/H_2 mixture. The values of the selectivity are comparable to the ones observed in MOFs and display a similar pressure dependence. The idealized models underestimate $S(\text{CO}_2/\text{H}_2)$ by about 15%.

The results presented in this paper pave the way for a systematic investigation of the properties of PGOF as a function of the density of pillars and the specific moiety used as a spacer. We showed how the results obtained with idealized models follow closely the results obtained with more realistic structures, generated using expensive ab initio calculations, with the proviso that the measured properties (such as adsorbed amounts or selectivity) can be up to 15% different from the actual ones.

ASSOCIATED CONTENT

Supporting Information

Coordinate file for the structure shown in Figure 1 in XYZ format. The unit cell is orthorhombic with sides of length 44.0, 42.0, and 39.2 Å. This material is available free of charge via the Internet at <http://pubs.acs.org>.

AUTHOR INFORMATION

Corresponding Authors

*E-mail: garberoglio@ectstar.eu.

*E-mail: taioli@ectstar.eu.

Notes

The authors declare no competing financial interest.

ACKNOWLEDGMENTS

The research leading to these results has received funding from the European Union Seventh Framework Programme under grant agreement n. 604391 Graphene Flagship. G.G. and S.T. acknowledge support by Istituto Nazionale di Fisica Nucleare through the “Supercalcolo” agreement with Fondazione Bruno Kessler. S.T. acknowledges economical support from the European Science Foundation under the INTELBIOMAT Exchange Grant “Interdisciplinary Approaches to Functional Electronic and Biological Materials” and the Bruno Kessler Foundation (FBK) for providing economical support through the “research mobility scheme” under which this work has been accomplished. Furthermore, S.T. gratefully acknowledges the Institute of Advanced Studies in Bologna for the support given under his ISA research fellowship and the high-performance computing service (PSMN) at the ENS de Lyon. N.M.P. is supported by the European Research Council (ERC StG Ideas 2011 BIHSNAM n. 279985 on Bio-Inspired hierarchical supernanomaterials, ERC PoC 2013-1 REPLICIA2 n. 619448 on Large-area replication of biological antiadhesive nano-surfaces, ERC PoC 2013-2 KNOTOUGH n. 632277 on Supertough knotted fibers), by the European Commission under the Graphene Flagship (WP10 “Nanocomposites”, n. 604391) and by the Provincia Autonoma di Trento (“Graphene Nanocomposites”, n. S116/2012-242637 and delib. reg. n. 2266). GCMC computer simulations were performed on the KORE computing cluster at Fondazione Bruno Kessler.

REFERENCES

- (1) Liao, L.; Lin, Y.-C.; Bao, M.; Cheng, R.; Bai, J.; Liu, Y.; Qu, Y.; Wang, K. L.; Huang, Y.; Duan, X. High-Speed Graphene Transistors with a Self-Aligned Nanowire Gate. *Nature* **2010**, *467*, 305–308.
- (2) Lin, Y.; Valdes-Garcia, A.; Han, S.-J.; Farmer, D. B.; Meric, I.; Sun, Y.; Wu, Y.; Dimitrakopoulos, C.; Grill, A.; Avouris, P. Wafer-Scale Graphene Integrated Circuit. *Science* **2011**, *332*, 1294–1297.
- (3) Cheng, R.; Bai, J.; Liao, L.; Zhou, H.; Chen, Y.; Liu, L.; Lin, Y.-C.; Jiang, S.; Huang, Y.; Duan, X. High-Frequency Self-Aligned Graphene Transistors with Transferred Gate Stacks. *Proc. Natl. Acad. Sci. U.S.A.* **2012**, *109*, 11588–11592.
- (4) Taioli, S.; Umari, P.; De Souza, M. Electronic Properties of Extended Graphene Nanomaterials from GW Calculations. *Phys. Status Solidi (b)* **2009**, *246*, 2572–2576.
- (5) Umari, P.; Petrenko, O.; Taioli, S.; De Souza, M. Communication: Electronic Band Gaps of Semiconducting Zig-Zag Carbon Nanotubes from Many-Body Perturbation Theory Calculations. *J. Chem. Phys.* **2012**, *136*, 181101.
- (6) Haberer, D.; Vyalikh, D. V.; Taioli, S.; Dora, B.; Farjam, M.; Fink, J.; Marchenko, D.; Pichler, T.; Ziegler, K.; Simonucci, S.; et al. Tunable Band Gap in Hydrogenated Quasi-Free-Standing Graphene. *Nano Lett.* **2010**, *10*, 3360–3366.
- (7) Haberer, D.; Petaccia, L.; Farjam, M.; Taioli, S.; Jafari, S. A.; Nefedov, A.; Zhang, W.; Calliari, L.; Scarduelli, G.; Dora, B.; et al. Direct Observation of a Dispersionless Impurity Band in Hydrogenated Graphene. *Phys. Rev. B* **2011**, *83*, 165433.
- (8) Henwood, D.; Carey, J. D. Ab Initio Investigation of Molecular Hydrogen Physisorption on Graphene and Carbon Nanotubes. *Phys. Rev. B* **2007**, *75*, 245413.
- (9) Ghosh, A.; Subrahmanyam, K. S.; Krishna, K. S.; Datta, S.; Govindaraj, A.; Pati, S. K.; Rao, C. N. R. Uptake of H₂ and CO₂ by Graphene. *J. Phys. Chem. C* **2008**, *112*, 15704–15707.
- (10) Ma, J.; Michaelides, A.; Alfè, D.; Schimka, L.; Kresse, G.; Wang, E. Adsorption and Diffusion of Water on Graphene from First Principles. *Phys. Rev. B* **2011**, *84*, 033402.
- (11) Tozzini, V.; Pellegrini, V. Prospects for Hydrogen Storage in Graphene. *Phys. Chem. Chem. Phys.* **2013**, *15*, 80–89.
- (12) Dreyer, D. R.; Park, S.; Bielawski, C. W.; Ruoff, R. S. The Chemistry of Graphene Oxide. *Chem. Soc. Rev.* **2010**, *39*, 228–240.
- (13) Joshi, R. K.; Carbone, P.; Wang, F. C.; Kravets, V. G.; Su, Y.; Grigorieva, I. V.; Wu, H. A.; Geim, A. K.; Nair, R. R. Precise and Ultrafast Molecular Sieving Through Graphene Oxide Membranes. *Science* **2014**, *343*, 752–754.
- (14) Cui, S.; Zhao, N.; Shi, C.; Feng, C.; He, C.; Li, J.; Liu, E. Effect of Hydrogen Molecule Dissociation on Hydrogen Storage Capacity of Graphene with Metal Atom Decorated. *J. Phys. Chem. C* **2014**, *118*, 839–844.
- (15) Chan, Y.; Hill, J. M. Hydrogen Storage Inside Graphene-Oxide Frameworks. *Nanotechnology* **2011**, *22*, 305403.
- (16) Burrell, J. W.; Gadipelli, S.; Ford, J.; Simmons, J. M.; Zhou, W.; Yildirim, T. Graphene Oxide Framework Materials: Theoretical Predictions and Experimental Results. *Angew. Chem., Int. Ed.* **2010**, *49*, 8902–8904.
- (17) Srinivas, G.; Burrell, J. W.; Ford, J.; Yildirim, T. Porous Graphene Oxide Frameworks: Synthesis and Gas Sorption Properties. *J. Mater. Chem.* **2011**, *21*, 11323–11329.
- (18) Kumar, R.; Suresh, V. M.; Maji, T. K.; Rao, C. N. R. Porous Graphene Frameworks Pillared by Organic Linkers with Tunable Surface Area and Gas Storage Properties. *Chem. Commun.* **2014**, *50*, 2015–2017.
- (19) Tang, Q.; Zhou, Z.; Chen, Z. Graphene-Related Nanomaterials: Tuning Properties by Functionalization. *Nanoscale* **2013**, *5*, 4541–4583.
- (20) Li, H.; Eddaoudi, M.; O’Keefe, M.; Yaghi, O. Design and Synthesis of an Exceptionally Stable and Highly Porous Metal-Organic Framework. *Nature* **1999**, *402*, 276–278.
- (21) Babarao, R.; Jiang, J. Molecular Screening of Metal-Organic Frameworks for CO₂ Storage. *Langmuir* **2008**, *24*, 6270–6278.
- (22) Wilmer, C. E.; Leaf, M.; Lee, C. Y.; Farha, O. K.; Hauser, B. G.; Hupp, J. T.; Snurr, R. Q. Large-Scale Screening of Hypothetical Metal-Organic Frameworks. *Nature Chem.* **2012**, *4*, 83–89.
- (23) Lin, L.-C.; Berger, A. H.; Martin, R. L.; Kim, J.; Swisher, J. A.; Jariwala, K.; Rycroft, C. H.; Bhowm, A. S.; Deem, M. W.; Haranczyk, M. In Silico Screening of Carbon-Capture Materials. *Nat. Mater.* **2012**, *11*, 633–641.
- (24) Düren, T.; Sarkisov, L.; Yaghi, O.; Snurr, R. Design of New Materials for Methane Storage. *Langmuir* **2004**, *20*, 2683–2689.
- (25) Düren, T.; Bae, Y.-S.; Snurr, R. Q. Using Molecular Simulation to Characterise Metal-Organic Frameworks for Adsorption Applications. *Chem. Soc. Rev.* **2009**, *38*, 1237–1247.
- (26) Getman, R. B.; Bae, Y.-S.; Wilmer, C. E.; Snurr, R. Q. Review and Analysis of Molecular Simulations of Methane, Hydrogen, and Acetylene Storage in Metal–Organic Frameworks. *Chem. Rev.* **2011**, *112*, 703–723.
- (27) Nicolai, A.; Zhu, P.; Sumpster, B. G.; Meunier, V. Molecular Dynamics Simulations of Graphene Oxide Frameworks. *J. Chem. Theory Comput.* **2013**, *9*, 4890–4900.
- (28) Nicolai, A.; Sumpster, B. G.; Meunier, V. Tunable Water Desalination Across Graphene Oxide Framework Membranes. *Phys. Chem. Chem. Phys.* **2014**, *16*, 8646–8654.
- (29) Hummers, W.; Offeman, R. Preparation of Graphitic Oxide. *J. Am. Chem. Soc.* **1958**, *80*, 1339–1339.
- (30) Pei, S.; Cheng, H.-M. The Reduction of Graphene Oxide. *Carbon* **2012**, *50*, 3210–3228.
- (31) Bagri, A.; Mattevi, C.; Acik, M.; Chabal, Y. J.; Chhowalla, M.; Shenoy, V. B. Structural Evolution During the Reduction of Chemically Derived Graphene Oxide. *Nature Chem.* **2010**, *2*, 581–587.

- (32) Kumar, P. V.; Bernardi, M.; Grossman, J. C. The Impact of Functionalization on the Stability, Work Function, and Photoluminescence of Reduced Graphene Oxide. *ACS Nano* **2013**, *7*, 1638–1645.
- (33) Assfour, B.; Seifert, G. Hydrogen Adsorption Sites and Energies in 2D and 3D Covalent Organic Frameworks. *Chem. Phys. Lett.* **2010**, *489*, 86–91.
- (34) Assfour, B.; Leoni, S.; Seifert, G. Hydrogen Adsorption Sites in Zeolite Imidazolate Frameworks ZIF-8 and ZIF-11. *J. Phys. Chem. C* **2010**, *114*, 13381–13384.
- (35) Zhou, W.; Wu, H.; Yildirim, T. Structural Stability and Elastic Properties of Prototypical Covalent Organic Frameworks. *Chem. Phys. Lett.* **2010**, *499*, 103–107.
- (36) Lukose, B.; Supronowicz, B.; Petkov, P.; Frenzel, J.; Kuc, A.; Seifert, G.; Vayssilov, G.; Heine, T. Structural Properties of Metal-Organic Frameworks Within the Density-Functional Based Tight-Binding Method. *Phys. Status Solidi (b)* **2012**, *249*, 335–342.
- (37) Garberoglio, G.; Taioli, S. Modeling Flexibility in Metal-Organic Frameworks: Comparison Between Density-Functional Tight-Binding and Universal Force Field Approaches for Bonded Interactions. *Microporous Mesoporous Mater.* **2012**, *163*, 215–220.
- (38) Hanwell, M. D.; Curtis, D. E.; Lonie, D. C.; Vandermeersch, T.; Zurek, E.; Hutchison, G. R. Avogadro: An Advanced Semantic Chemical Editor, Visualization, and Analysis Platform. *J. Cheminformatics* **2012**, *4*, 17.
- (39) Halgren, T. Merck Molecular Force Field. I. Basis, Form, Scope, Parameterization, and Performance of MMFF94. *J. Comput. Chem.* **1996**, *17*, 490. See also the three subsequent papers in the same journal issue.
- (40) Aradi, B.; Hourahine, B.; Frauenheim, T. DFTB+, a Sparse Matrix-Based Implementation of the DFTB Method. *J. Phys. Chem. A* **2007**, *111*, 5678–5684. <http://www.dftb-plus.info/>
- (41) Kresse, G.; Hafner, J. Ab Initio Molecular Dynamics for Liquid Metals. *Phys. Rev. B* **1993**, *47*, 558.
- (42) Alfe, D. Ab Initio Molecular Dynamics, a Simple Algorithm for Charge Extrapolation. *Comput. Phys. Commun.* **1999**, *118*, 31–33.
- (43) Perdew, J. P.; Burke, K.; Ernzerhof, M. Generalized Gradient Approximation Made Simple. *Phys. Rev. Lett.* **1996**, *77*, 3865.
- (44) Lukose, B.; Kuc, A.; Frenzel, J.; Heine, T. On the Reticular Construction Concept of Covalent Organic Frameworks. *Beilstein J. Nanotechnol.* **2010**, *1*, 60.
- (45) Buch, V. Path Integral Simulations of Mixed *Para*-D₂ and *Ortho*-D₂ Clusters: The Orientational Effects. *J. Chem. Phys.* **1994**, *100*, 7610–7629.
- (46) Harris, J.; Yung, K. Carbon Dioxide's Liquid-Vapor Coexistence Curve and Critical Properties As Predicted by a Simple Molecular Model. *J. Phys. Chem.* **1995**, *99*, 12021.
- (47) Mayo, S.; Olafson, B.; Goddard, W., III DREIDING: A Generic Force Field for Molecular Simulations. *J. Phys. Chem.* **1990**, *94*, 8897.
- (48) Rappé, A.; Casewit, C.; Colwell, K.; Goddard, W., III; Skiff, W. UFF, a Full Periodic Table Force Field for Molecular Mechanics and Molecular Dynamics Simulations. *J. Am. Chem. Soc.* **1992**, *114*, 10024.
- (49) Garberoglio, G.; Skoulidas, A.; Johnson, J. Adsorption of Gases in Metal Organic Materials: Comparison of Simulations and Experiments. *J. Phys. Chem. B* **2005**, *109*, 13094–13103.
- (50) Sumida, K.; Rogow, D. L.; Mason, J. A.; McDonald, T. M.; Bloch, E. D.; Herm, Z. R.; Bae, T.-H.; Long, J. R. Carbon Dioxide Capture in Metal-Organic Frameworks. *Chem. Rev.* **2011**, *112*, 724–781.
- (51) Feynman, R.; Hibbs, A. *Quantum Mechanics and Path-Integrals*; McGraw-Hill: New York, 1965.
- (52) Wang, Q.; Johnson, J. K.; Broughton, J. Q. Path Integral Grand Canonical Monte Carlo. *J. Chem. Phys.* **1997**, *107*, 5108.
- (53) Garberoglio, G. Boltzmann Bias Grand Canonical Monte Carlo. *J. Chem. Phys.* **2008**, *128*, 134109.
- (54) Garberoglio, G.; Johnson, J. Hydrogen Isotope Separation in Carbon Nanotubes: Calculation of Coupled Rotational and Translational States at High Densities. *ACS Nano* **2010**, *4*, 1703.
- (55) Garberoglio, G. Quantum Effects on Virial Coefficients: A Numerical Approach Using Centroids. *Chem. Phys. Lett.* **2012**, *525*–526, 19.
- (56) Rouquerol, J.; Rouquerol, F.; Llewellyn, P.; Maurin, G.; Sing, K. S. *Adsorption by Powders and Porous Solids: Principles, Methodology and Applications*; Academic press: New York, 2013.
- (57) Garberoglio, G. Computer Simulation of the Adsorption of Light Gases in Covalent Organic Frameworks. *Langmuir* **2007**, *23*, 12154–12158.
- (58) Walton, K. S.; Millward, A. R.; Dubbeldam, D.; Frost, H.; Low, J. J.; Yaghi, O. M.; Snurr, R. Q. Understanding Inflections and Steps in Carbon Dioxide Adsorption Isotherms in Metal-Organic Frameworks. *J. Am. Chem. Soc.* **2008**, *130*, 406–407.
- (59) Li, J.-R.; Ma, Y.; McCarthy, M. C.; Sculley, J.; Yu, J.; Jeong, H.-K.; Balbuena, P. B.; Zhou, H.-C. Carbon Dioxide Capture-Related Gas Adsorption and Separation in Metal-Organic Frameworks. *Coord. Chem. Rev.* **2011**, *255*, 1791–1823.
- (60) Yang, Q.; Zhong, C. Molecular Simulation of Carbon Dioxide/Methane/Hydrogen Mixture Adsorption in Metal-Organic Frameworks. *J. Phys. Chem. B* **2006**, *110*, 17776–17783.
- (61) Yang, Q.; Xu, Q.; Liu, B.; Zhong, C.; Berend, S. Molecular Simulation of CO₂/H₂ Mixture Separation in Metal-Organic Frameworks: Effect of Catenation and Electrostatic Interactions. *Chin. J. Chem. Eng.* **2009**, *17*, 781–790.
- (62) Battisti, A.; Taioli, S.; Garberoglio, G. Zeolitic Imidazolate Frameworks for Separation of Binary Mixtures of CO₂, CH₄, N₂ and H₂: A Computer Simulation Investigation. *Microporous Mesoporous Mater.* **2011**, *143*, 46.